[1] Haichuan Zhang [1],
Yuchuan Zhang [2*],
Haibo Wang [3],
Yu Ao [4]

Enhanced Microwave Beam Synthesis for Phased Array Antennas in High Power Applications

Journal of Electrical Systems

Abstract: - This paper presents advanced methodologies for enhancing microwave beam synthesis in phased array antennas used in high-power applications. The research focuses on optimizing key parameters such as array configuration, excitation amplitude, and phase control to achieve more precise and powerful beamforming. Novel beam synthesis algorithms are developed to increase the efficiency of energy delivery while minimizing beam distortions and power losses. The study also compares the performance of various array architectures in high-power scenarios, providing a comprehensive analysis of how phased arrays can be optimized for robust beam synthesis. The findings offer valuable guidelines for improving high-power microwave transmission methods.

Keywords: Microwave beam synthesis, phased array antennas, high-power applications, beamforming, array configuration, energy efficiency, beam optimization.

1. Introduction:

For the past four to five decades, active phased array antenna units (AAAUs) have been state-of-the-art. Over the past two decades, research and development efforts in India have been centred on AAAUs, garnering significant attention. LRDE is a leading organisation in India that strives to supply active phased array antenna solutions for various platforms, including military and civilian ones, for radar applications within the nation. In the past, different LRDE initiatives have made use of semiconductor methods such GaAS, BJT, LDMOS, Si, etc. Yet, these technologies' power output, heat dissipation, power added efficiency (PAE) are severely constrained in higher frequency bands (>S-band). From this point forward, bigger apertures with a high number of active radiating elements are needed to provide the necessary power-aperture (ERP) product [1]. This has significant consequences for the cost and dependability of active phased array antennas. It also increases need for cooling since there is a greater need for large DC power input as well as large volume of active electronics, particularly transmit-receive models. It makes SWAP-C higher. Wide bandgap GaN technology's introduction has created a number of opportunities for achieving greater ERP with smaller apertures. An antenna functions as a transducer and is utilized to send and receive electromagnetic (EM) waves. Each component that makes up an antenna array operates within its own induction field. Better radiation can be produced via an antenna array. The antenna array can be used to boost the directivity, which produces a strong signal in a particular direction. One of the printed antennas that is most frequently utilised in wireless applications is the microstrip patch antenna (MSPA). It is mostly utilised because of its benefits, which include its ease of production and its adaptability to any shape. The radiation pattern produced by an array antenna is equal to vector sum of radiation patterns produced by every element in array because it can give higher gain as well as directivity than a single antenna. Military communications, radar, and satellite applications are the main uses for antenna arrays [2]. An antenna array's characteristics are determined by how individual elements are arranged, how much current is flowing through them, how each element is activated by a progressive phase change. An antenna array is typically utilized in point-to-point transmission. Through the use of microwaves in free space, Microwave Wireless Power Transmission (MWPT) transfers radio frequency (RF) power and subsequently transforms it into direct current (DC) power without the need for physical wires or connections. For instance, solar energy is transferred from orbit to Earth's surface [3] and subsequently transformed into electrical power. Remote highlands and other

[1] Northwest Institute of Nuclear Technology, Xi'an, Shanxi, 230037, China

E-Mail: zhanghai4258@163.com

Corresponding Author: **Yuchuan Zhang**

Northwest Institute of Nuclear Technology, Xi'an, Shanxi, 230037, China

E-Mail: zhanghai4258@163.com

locations with challenging environmental conditions receive electricity from offshore wind turbines. MWPT offers an advantage over other wireless power transmission methods, such as magnetic resonance and electromagnetic coupling, because of its large transmission distance. Utilising this technology has recently aided in the advancement of wireless charging, green radio communications, and microsystem power supplies. Early on, extensive research on long-distance, high-power MWPT methods was conducted in United States. Tesla finished the first microwave wireless energy transmission experiment in 1899. An important long-distance microwave phase transition (MWPT) experiment was conducted by Jet Propulsion Laboratory (JPL) in 1957. The experiment was conducted at an operating frequency of 2.388 GHz over a transmission distance of 1.6 km in the Mohave Desert. Experiment effectively obtained 30 kW DC power while transmitting 450 kW of microwave power [4]. Levitation device was powered by wireless microwave radiation as well as operated for ten hours at a height of fifty feet thanks to a platform that W. Brown erected in 1964. Over time, academics in Europe and Japan have been increasingly interested in MWPT. In 1992, the vehicle and the aeroplane exchanged microwave signals, and beam scanning was used to track the aircraft's position. In transmit/receive modules used in microwave and radio frequency (RF) systems, a phase shifter is an essential part. Phase discriminators, beam-switching arrays, balanced RF amplifiers, microwave power dividers, BFNs (Beam-forming Networks), and other equipment types find significant uses for it. An extensive number of antenna elements that radiate signals to produce a concentrated electromagnetic beam define a phased antenna array. The primary characteristic of a phased array antenna is its capacity to actively modify relative phases of individual antenna elements in order to electrically control the radio beam's direction [5]. This capability is made possible by phase shifters, which are essential for beam scanning and shape reconfiguration. Phased antenna arrays are made up of several separate components in real-world applications, such as aircraft TCAS (Traffic Collision Avoidance System) antennas. To apply the necessary phase shift—which is crucial for directing the antenna beam—each of these components needs its own phase shifter. Furthermore, a phase shifter is employed in certain avionics systems that use amplitude mono pulse techniques to transition between various directional and Omni-directional antenna modes. In conclusion, phase-shifters play a crucial role in radiofrequency and microwave systems, particularly in phased array antennas, where they allow for fine control and modification of the direction and shape of the antenna beam for uses like avionics and radar systems [6].

2. Related works:

Numerous reports of optically controlled phased arrays have surfaced in recent decades. For the first time, an optical-fiber-based completely functional millimeter-wave array with a real time delay was demonstrated by authors in [7]. Antennas had an incredibly broad working bandwidth and were intended to operate in the 1–50 GHz range. The microwave device being used was the only factor limiting the antenna's bandwidth. The authors showcased an antenna array with exceptional beam-scanning capabilities that might span the whole Ka band. An optical phased array antenna with a broadband operational bandwidth was proposed by the authors in [8]. The unit of the planned phased array was a broadband Vivaldi antenna. Some instructors have been presenting alternative approaches that resemble the one in [9] in recent years. They replace the dielectric sheet in [10] with a SRRs (sheet of split-ring resonators), multilayer WAIM structure, 2 layer WAIM structure, a metamaterial slab, frequency select surface to realize wide-angle scanning capabilities of array antenna. SICB (Substrate-integrated cavity-backed) structure [11], high impedance surfaces (HIS), DGS (defective ground structure), EBG (electromagnetic band gap) structure are used to reduce surface waves and enhance WAIM. It is not a novel idea to guide antenna main lobe by varying excitation signal's frequency. Frequency beam-steering arrays typically feed the radiating elements through series feeding networks. Designing feeding network might be based on linked lines, substrate integrated waveguides (SIWs), or traditional waveguides [12]. Regretfully, applying synthesis at a series feeding network is quite complex. This problem reduces a WPT system's efficiency since more electrical energy is lost far from equivalent Rx rectenna the greater SLL at Tx side. A small number of documented designs have successfully surmounted this difficulty, such as [13], where series-feed antenna arrays were able to reach −19 dB SLL at sacrifice of antenna efficiency. Furthermore, parallel-feed networks have been utilised to frequency beam-steering antenna arrays in a few other documented systems [14]. Sadly, these designs' complex multilayer structures and high SLL and/or low radiation efficiency (50%) are their downfalls. Tx antenna should have a good power handling capability in long-range WPT. Antenna peak power capacity has been increased using a variety of approaches. While leaky waveguide antennas published in [16]

may manage up to a few gigawatts, radial line helical antenna arrays presented in [15] can sustain a peak power of various megawatts. For high power applications, a reconfigurable bent horn antenna was suggested in [17]. None of these earlier high power devices were able to take advantage of beamforming. A high power phased antenna array was suggested later in [18]. Despite its effective high power beam steering, its use in a WPT method is restricted because its phase shifters are managed by active servomotors.

3. SUBARRAY DESIGN

Following is a summary of the essential design factors that must be met for every subarray based on the design idea. A. Unidirectional Radiation with High Gain (Gmax ≥ 10 dBi and FBR ≥ 10 dB) B. Coverage in Quarter Hespherical s (ηc ≥ 0.7 for Gth > 8 dBi) a. Azimuth Steered Beam (for −45◦ ≥ φ ≥ +45◦) b. Elevation Wide Inclined Beam (for 0◦ ≥ θ ≥ +90◦) C. Small and Low-Profile Design D. Sufficient Reflection Coefficients as well as Mutual Couplings (≤ −10 dB throughout 28 GHz – 29 GHz frequency range). We supply array after describing design of antenna elements. Radiation pattern of a complimentary dipole antenna and an ideal narrow slot placed into an infinitely conducting sheet is the same, but the E- and H-fields are flipped. When half-wavelength slit is put into infinite flat sheet at z = 0 is pointing in x direction, electric field patterns at far-field observation sites are identified as follows by eqn (1)

$$E(\theta) = \mathrm{A}\left[\frac{\cos(\pi/2\cos\theta)}{\sin\theta}\right], \text{ for } \phi = 0^{\circ}$$

$$E(\theta) = \mathrm{A}, \text{ for } \phi = 90^{\circ} \quad (1)$$

where the constant is A. With infinite sheet dimensions, the optimal λ/2 slot antenna radiates in both directions: nondirectionally in yz-plane (E-plane) and bidirectionally in xz-plane (H-plane). At far-field observations, slot antenna with finite sheet dimensions' E-plane electric-field pattern is theoretically approximated by eqn (2)

$$|E_{EP}(\theta)| \approx \sqrt{1 + 4b\cos\beta d\cos(\beta d\sin\theta)}, \text{ for } \phi = 90^{\circ} \quad (2)$$

where d is distance between slot aperture and sides, wave number at 28 GHz. In yz-plane (E-plane) proposed slot antenna has a quasi-nondirectional pattern, while in xz-plane (H-plane) it is bidirectional, in contrast to perfect slot antenna.

Microstrip Patch Antenna Array. RT/Duroid 5880 substrate is utilized in creation of the -shaped MSPA antenna arrays, measuring 2 × 2 and 3 × 3. 2.4 GHz is the design frequency. Substrate material has a thickness of 3 mm. Formula below is used to design width and length of the microstrip patch antenna array (MSPAA). Then, ADS software is utilized to method suggested antenna array design. For 2 × 2 and 3 × 3 antenna arrays, performance characteristics like gain, directivity, and return loss are mentioned. Suggested system is designed utilizing procedures listed below. Width (W) of antenna array is calculated by eqn.(3)

$$w = \frac{c}{2f_0\sqrt{\frac{(e_S+1)}{2}}} \quad (3)$$

Effective dielectric constant evaluation is represented by eqn (4)

$$\varepsilon_{\mathrm{eff}} = \frac{\varepsilon_{\mathrm{r}}+1}{2} + \frac{\varepsilon_{\mathrm{r}}-1}{2}\left[\frac{1}{\sqrt{\left(1+12\frac{h}{W}\right)}}\right] \quad (4)$$

Effective length is evaluated by eqn (5)

$$L_{\mathrm{eff}} = \frac{c}{2f_0\sqrt{\varepsilon_{\mathrm{eff}}}} \quad (5)$$

The length extension ΔL is given by eqn (6)

$$\Delta L = 0.412h\frac{(\varepsilon_{\mathrm{eff}}+0.3)\left(\frac{W}{h}+0.264\right)}{(\varepsilon_{\mathrm{eff}}-0.258)\left(\frac{W}{h}+0.8\right)} \quad (6)$$

Actual length of patch is as follows $L = L_{\mathrm{eff}} - 2\Delta L$

As seen in Figure 1, the entire phased array was made up of an optical network module, a transmitting/receiving (T/R) module, and a passive antenna. The T/R module was made up of an electrical time-delay module and a microwave amplifier with circulator, power amplifier, low-noise amplifier, switching method that could separate transmitting as well as receiving connections. Unvisible in the illustration, a beam controller managed the phase shifting of every channel. First, each component was divided into functional modules using a modular framework, which also allowed the hardware structure to be independently assembled and tested. Ultimately, every component was put together and merged using matching interface relations to create entire antenna array. This simplified assembly process as well as made it easier to evaluate the module's physical structure.

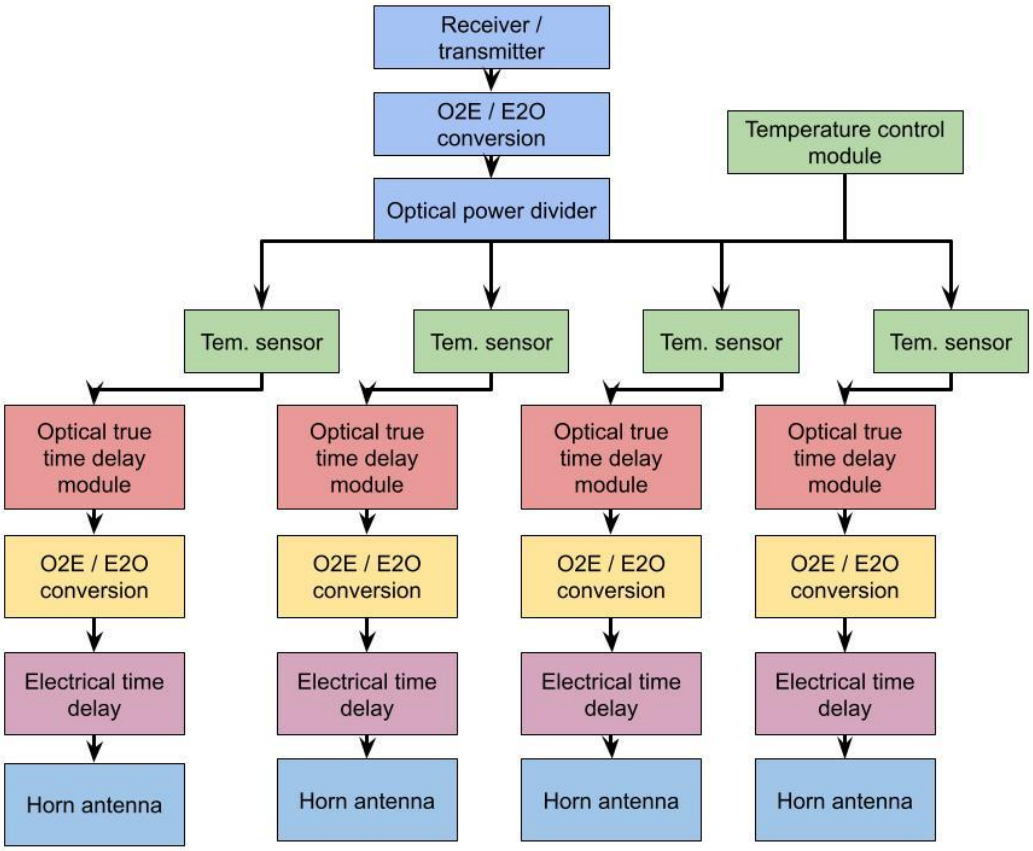

Figure 1. A schematic diagram of microwave-photonics-based broadband phased array.

The antenna element of phased array was selected to be a horn antenna. The microwave signal was received and delivered from free space. The TR module had the antennas attached to it. The two amplifiers that were part of TR model were a power amplifier as well as low-noise amplifier. Power amplifier was in charge of amplifying the transmitted microwave signal, while the low-noise amplifier amplified the received microwave signal. Using receiving connection as an example, electro-optical conversion module transformed microwave signal into an optical signal. Optical model delay line then phase-shifted optical signal to reveal phase difference between every unit. The optical power divider combined several phase-shifted optical signals to create a single optical-band received signal. Optical signal then went via the photoelectric conversion module to become a microwave signal, which was then sent to microwave receiver for further processing. This was same process, but signal flow was different in transmitting link.

It should be mentioned that we combined an electronic and optical time delay into a hybrid solution for this design. This plan made it possible to benefit from both the little electronic time delay and big optical fibre time delay. It was able to increase beam-pointing precision and offer wide-angle scanning, both of which are critical in radar application settings. Each antenna, as seen in Figure 1, was attached to an electronic time delay at back end, which was utilised to suitably delay broadcast or reception. Signal entered optoelectronic/electro-optical converter module, delayed by optical time delay, after passing through the power divider and T/R module.

Antenna thus accomplished one-dimensional beam scanning, that is, beam scanning perpendicular to direction where optical time delays are arranged.

The element interval was established at 42.8 mm, or 0.82λ. After attaching coaxial components that simulated SMA connectors behind MSAs, signals were stimulated using waveguide ports that included the phases and amplitudes that were designed in Section II. Furthermore, to excite same flat-top beam with less elements, an additional array model was constructed. Excitation power levels were more than 30 dB lower in third and fourteenth rows (x-axis) and third and fourteenth columns (y-axis) than in centre elements. It is assumed that the components in those lines have no effect on the flat-top beam's resulting radiation pattern. As a result, the second array model did not include those elements. Designing distribution circuits will be simpler due to the decrease in the number of elements. 16-by-16-element array and 14-by-14-element array's power density patterns were examined at a 1 W total transmitted power. Beam patterns as well as power levels were nearly identical in those two, as this image illustrates. Therefore, in order to streamline the distribution circuit design, phased array to be created in subsequent sections is a 14-by-14-element array. For a more comprehensive understanding, were used to determine variations in beam efficiency as well as CV of a radiated flat-top beam with regard to varied threshold values for element elimination by eqn (7).

$$p_{\mathrm{d}}(x,y,z) = P_{\mathrm{T}} F(x,y,z)^2$$

$$F(x,y,z) = \mathrm{C}\sum_{m=1}^{M}\sum_{n=1}^{N} |E(\theta,\phi)| w_{m,n} \exp\left(-jkr_{m,n}\right)/\sqrt{4\pi} r_{m,n}$$

$$\mathrm{C} = \sqrt{\left(\sum_{m=1}^{M}\sum_{n=1}^{N} \left|w_{m,n}\right|^2 \int_0^{2\pi}\int_0^{\pi} |E|^2 d\theta d\phi\right) / \left(\int_0^{2\pi}\int_0^{\pi} |E|^2 \left|\sum_{m=1}^{M}\sum_{n=1}^{N} w_{m,n} \exp\left(jkp_{m,n}\cdot \boldsymbol{r}\right)\right|^2 d\theta d\phi\right)} \quad (7)$$

Despite the fact that the element simulations produced an excellent axial ratio of 0.34 dB, axial ratio was greater than 3 dB over whole receiving area. This degradation was most likely brought about by unfavourable mutual interaction between the components. Techniques for successive arrays were used to increase the axial ratio. In the traditional technique, each array's antenna element is physically turned 90 degrees anticlockwise, and in the case of RHCP, the injected signal's phase is electrically delayed by 90 degrees. Mutual coupling effect can be eliminated while preserving the array antenna's beam emission pattern thanks to these electrical and physical phase rotations. Distributing the proper amplitude as well as phase to every antenna element while taking into account electrical phase delays for each element as well as physical rotation of the feeding pins is challenging, though. Distribution circuit design is quite complex due to this necessity. Instead of rotating the 196-element array element by element, each of the four subarray blocks that make up this division is rotated 90 degrees anticlockwise to the adjacent blocks. In the upcoming parts, the distribution circuit design will be much simpler thanks to this design technique, which we refer to as block-oriented sequential array. All we need to do is set up four identical 49-way distribution circuit pieces with antennas, place them on the same plane and rotate them 90 degrees counterclockwise to each other, and then provide each block with four signals with a different phase delay (0, 90, 180, and 270 degrees).

4. HIGH-POWER MICROWAVE FEED ANTENNA

In a microwave anechoic chamber, conventional power testing of feed antenna are conducted. Measured findings are compared with simulated results in Figure 2. Measured reflection coefficient, as depicted in Fig. 2(a), is less than −10 dB between 4.1 and 4.5 GHz, reaching a minimum of −24.9 dB at 4.37 GHz. Primary reason for discrepancy between simulated as well as measured values is machining and assembly error. The measured axial ratio from 4.15-4.4 GHz is less than 3 dB, as shown in Fig. 2(b), which is essentially compatible with simulation. Figures 2(c) and (d) show that rotational symmetry of radiation beam is excellent and that observed co-polarization and cross-polarization radiation patterns at 4.3 GHz agree well with simulation.

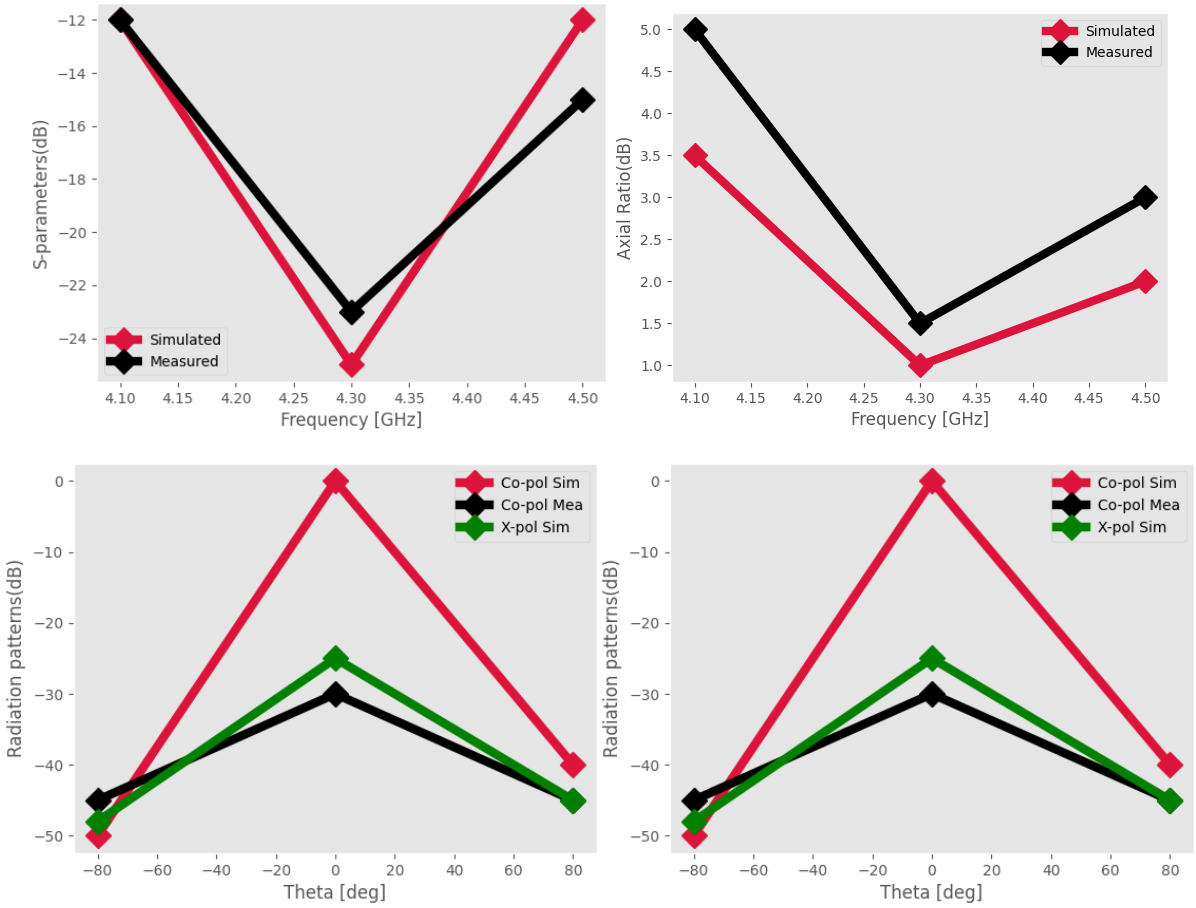

Figure 2. Performances of feed antenna. (a) S-parameters. (b) Axial ratio. (c) Radiation patterns at 4.3 GHz ($\phi 0 = 0^{\circ}$) and (d) ($\phi 0 = 90^{\circ}$).

First, a positioning plate with specific design is placed on the reflect array surface. The positioning plate's through-holes are laser-cut, rotation angle of every through-hole corresponds to distribution of rotation angles. The metal element's rotation angle can then be adjusted by sliding element fixator into positioning plate. Lastly, positioning plate should be removed and a random should be applied to the metal frame. By limiting the rotation angle error to within $\pm 0.5^{\circ}$, this technique improves consistency between the simulation and experimental results. The simulated and actual findings correlate well, and there is always a suppression of cross-polarization level below - 22 dB. Less than 0.14 dB separates simulated and measured gain. The minimum and maximum axial ratios during beam scanning are 0.35 dB and 1.23 dB.

Experimental findings demonstrate high aperture efficiency as well as good beam-steerable capacity of C-band WRA for future HPM investigations. Furthermore, Tx antenna array should radiate many primary lobes in a sequential, randomised, or simultaneous manner for various receivers. Active phase shifters are employed in phase beam-steering antenna arrays in order to direct the beam. As a result, phase changers require electrical energy to turn on and be controlled at Tx side. A WPT method efficiency is lowered as a result.

In order to minimise the amount of energy lost at side lobes, the SLL of transmit antenna array's radiation patterns are decreased, as goal of a WPT method is to provide greatest transmitted power to RX rectennas. Therefore, in order to reduce the SLL, synthesis needs to be applied to feeding network.

Since frequency beam-steering antenna arrays typically use series feeding networks. Therefore, in order to minimise SLL, this research presents a frequency beam-steering antenna array with a synthesised parallel feeding network, in contrast to other published designs in the prior works.

A frequency beam-steering antenna array's array factor, or AF, is described as eqn (8)

$$AF = \sum_{m=1}^{M} W_m e^{j(m-1)\left(\frac{2\pi}{\lambda} d\cos\theta - \frac{2\pi}{\lambda_g} S\right)} \quad (8)$$

Consequently, λ ≈ λg). When θ = θm, where, eqn (9) has its maximum value

$$\theta_m = \cos^{-1}\left(\frac{S\sqrt{\varepsilon_r}-n\lambda}{d}\right),\ n \text{ is a positive integer} \quad (9)$$

After applying (3) to set θm to 60° and 90° at 1.1 GHz and 1.5 GHz, respectively, S and d are found to be 340 mm and 140 mm. Suggested antenna element terminates each of the 16 output ports, creating a 16-element linear antenna array. The WPT system's efficiency will suffer as a result. 16 elements' phases decrease one after the other according to Δarg(Wm), which changes with wavelength and takes the form Δarg(Wm) = 2πS/λg.

A number of contributions from both internal and external noise sources are added up to determine the system noise temperature. Former is ground noise that has been picked up as a result of spillover and is calculated using the reflector's simulated illumination pattern, or the feed's primary pattern. The thermal antenna noise resulting from conductor material losses in TSAs and microstrip feeds is one of the two components that make up the internal noise contribution. By applying the methods to assess radiation efficiency of antenna, conductor losses are calculated.

Multi-channel receiver noise, which is computed using a system model of the comparable single-channel receiver. Antenna-LNA impedance noise mismatch effect as well as low noise of LNAs are explained by this noise component. This model uses the sky as a reference for the system noise temperature contribution. Analysing sensitivities at 1.2 GHz, 1.42 GHz, 1.6 GHz reveals the benefit of restricted optimisation in minimising sensitivity fluctuation over a broad field of view and frequency spectrum. To highlight the various shapes in these photos, they have been normalised to their maxima. With the MaxSNR beamformer, there is a 10% increase in absolute sensitivity at beam centres. The mean absolute values of sensitivity values for the beamformers under consideration, along with the associated maximum sensitivity ripple.

5. THE PERFORMANCE OF THE ARRAY ANTENNAS

Figure 3 illustrates analysis of simulated as well as measured reflection coefficients of E- and H-plane scanning array antennas. There is a rough agreement between measured as well as simulated findings. E-plane scanning array antenna's impedance bandwidth is 3.18 – 3.95 GHz (21.6%), whereas H-plane scanning array antenna's is 3.18 – 3.90 GHz (20.3%).

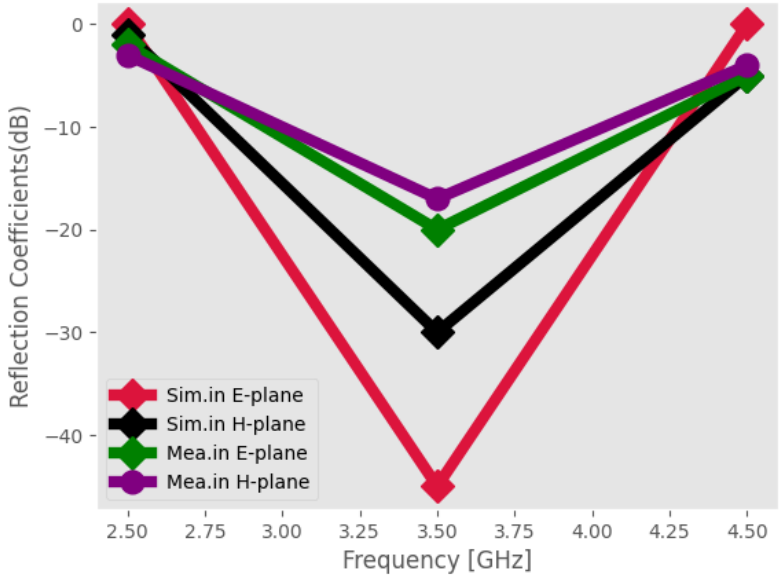

Figure 3. Measured and simulated reflection coefficients of array antennas.

Eq. (4) was used to calculate the normalised gain patterns for yz- and xz-planes using different values of h. When looking at both planes, the highest relative gain occurs at h = 0.25 λ in boresight direction (i.e., θ = 0 ◦). At some point, gain pattern spreads to both sides, as h increases between λ/4 and λ/2, the power at θ = 0 ◦ progressively decreases. In contrast, computed values in H-plane for those h values are, 136◦, 148◦, 152◦, and 154◦. Design parameter h is optimized at 0.4 λ, which yields broadest beamwidth and a significant gain at θ = 0.

Biggest relative improvement in this case happens at θ = ±37◦. If half of H-plane design were accurately deleted, given AMC-backed slot antenna would fulfill needed wide inclined elevation beam.

For array antenna to conduct wide-angle scanning with a gain fluctuation of less than 3dB, following conditions. First off, main beam of array antenna is negatively impacted by grating lobe of the array. Grating lobe of array must be muted. To suppress grating lobe, requirement is given by eqn (10)

$$d < \frac{\lambda}{1+|\sin\theta|}\left(1-\frac{1}{2N}\right) \tag{10}$$

Scanning angle is θ, inter-element spacing is d. Total number of antenna elements is N. Scanning angle in this study is up to 90◦, and N is 9. Thus, the distance between elements is given by eqn (11)

$$d < \frac{\lambda}{1+|\sin\theta|}\left(1-\frac{1}{2N}\right) \approx 0.47\lambda \tag{11}$$

The dielectric layer reduces the antenna element's size. 36 mm is the inter-element spacing, or 0.45 λ at 3.8 GHz. Equation (2) is satisfied by the inter-element spacing throughout the whole bandwidth. Additionally, even though the inter-element spacing stays constant, radiating patch of element fluctuates slightly and mutual coupling of antenna elements is moderately minimized. To ensure that gain change is less than 3dB while scanning a greater area, the array antenna must have a substantially wide beam-width. As so, the electric walls enlarge the beam of the broad beam antenna, which is then employed in array antennas.

To detect targets or convey messages to distant receivers, the main lobe is manoeuvred to an exact location or in close proximity to it within a tolerance error. Beam pointing error (BPE) can result from the system's intrinsic faults causing the primary lobe to steer to an undesirable location. One of the possible causes of this error could be the phase shifter's own RMS phase error or an error brought on by variations in the input radio frequency. The phase shifter's quantisation effect is another factor that raises the beam directing error. Variable attenuation and phase faults should not exist in the output of an ideal phase shifter. Beam steering commands are generated in MATLAB and sent to systemVue. The appropriate phase shifts are produced by the MATLAB code and are given to each individual DAC. The manufacturer's s2p file for selected MMIC DAC was utilized in simulations, relevant phase shifts and attenuation were added for an input signal of -20dBm for various DPS states. These were observed and recorded during the simulations.

$$\Delta_{\text{err}} = \pm 0.5\left(\Delta_{\text{err},\max} - \Delta_{\text{err},\min)}\right) = \pm 0.632 \tag{12}$$

RMS phase error, Ω_{err};

$$\Omega_{\text{err}} = \frac{\sqrt{\varphi^2}}{N} \tag{13}$$

It is computed that the average phase divergence with respect to the DPS frequency is - 97.03o /GHz.

Table 1. Scanning radiation performance with various directions at various frequencies in E-plane array

Frequency (GHz)	**3.2**		**3.5**		**3.8**	
	Gain (dBi)	**SLL (dB)**	**Gain (dBi)**	**SLL (dB)**	**Gain (dBi)**	**SLL (dB)**
-90	12.8	-12.4	13.2	-12.2	12.8	-10.0
-60	10.7	-3.0	11.5	-5.0	12.5	-8.7
-30	12.2	-9.5	12.5	-8.1	13.1	-6.0
0	13.5	-13.4	14.1	-11.6	14.8	-11.2
30	12.2	-9.5	12.5	-8.2	13.0	-6.1

60	10.8	-3.0	11.6	-5.1	12.4	-8.8
90	12.7	-12.0	13.2	-13.1	12.8	-10.0

The above array antenna's mimicking radiation patterns are provided at three different operational bandwidth frequencies. Throughout entire operational frequency range, antenna's beam can scan from -90◦ to +90◦ with a gain change of less than 3dB. Table 1 provides proposed antenna's comprehensive scanning performance. As the beam's scanning angle increases, gain of suggested antenna progressively drops. But when the scanning angle goes beyond sixty, the antenna's gain rises as the scanning angle changes. Furthermore, all of the scanning beam's SLLs—aside from the one at 60—are lower than 6.0 dB. Wide-angle scanning capability of array antenna is realised through application of suggested technology. The electric wall makes the antenna element's wide beam performance possible. Array antenna's gain is not particularly strong because its gain variation is less than 3 dB in beam scanning coverage from -90 to +90. Array antenna has lowest gains at 3.2 GHz, between 10.7 and 10.8 dBi, when the scanning angles are ±60◦.

6. Effect of Quantization Effect of Phase Shifter on Array Pattern

To attain the required side-lobe envelope as well as beam aiming accuracy, antenna synthesis is carried out. On the other hand, there are other possible causes of system errors. It is necessary to examine the margin of error during synthesis since quantisation errors might greatly increase the unwanted SLL envelope. To achieve the intended performance with the tolerances that the designer has pre-defined, it is crucial to select the right bits well in advance. In order to exclude random or uncontrollable errors in the end, it is a good idea to eliminate as many associated errors as feasible. It is important to take precautions to ensure that the specifications fall substantially below the tolerance margin once these faults are introduced.

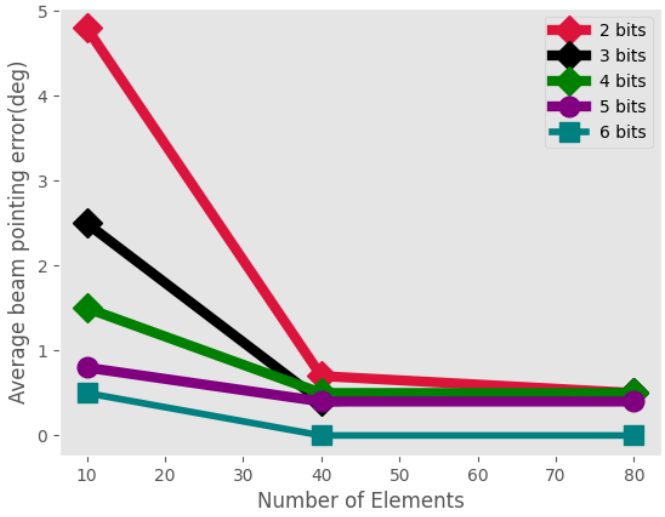

Figure 4. Variation of Average BPE v/s Number of Elements in the Array

The simulated 3D radiation patterns of the antenna array at the start, centre and stop frequencies are shown in Fig. 5 while the measured normalized radiation patterns in the E-plane at 1.1, 1.2, 1.3, 1.4 and 1.5 GHz. It is evident that the antenna array steers its main lobe in correspondence to the swept frequency of the feeding signal at a good agreement with the desired directions. It is also obvious that the measured peak SLL is better than −20 dB at any radiation pattern across the frequency band.

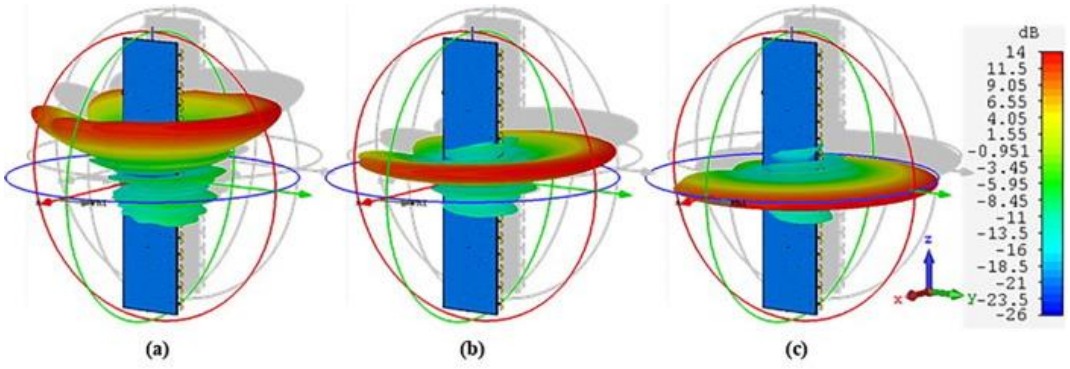

Figure 5. The 3D simulated radiation patterns of the antenna array at (a) 1.1 GHz (b) 1.3 GHz (c) 1.5 GHz. [19]

However, this does not imply that the designer needs to go out and get an extremely high bit phase shifter right away. Phase shifters in present T/R model that are simulated are flawless, providing an optimum radiation pattern. Additionally, phase shift weights that are produced are perfect. This indicates that they lack any means of compensating for quantisation errors that might arise in the real-world MMIC. To assess the antenna system's actual performance, these will be changed. When determining the DPS resolution, two primary factors are taken into account: BPE as well as ASLL and PSLL. BPE, or beam deviation, is simply angle measured by difference between intended main-lobe locations as well as actual location. It has been found that while the array's element count rises, the beam deviation falls. It may be inferred that as number of elements increases, beam deviation decreases. This indicates that beam formation can be done with relatively little beam deviation even with a low phase shifter resolution if array size is large enough. Figure 4 illustrates how BPE varies in relation to the number of elements. When array size is big, influence of quantisation mistake may not be as noticeable on BEP; nevertheless, issue becomes apparent when effect is noticed on array factor. Result of quantisation errors is a parasitic side-lobe. An unusually high side-lobe that results from an array factor error can be described as a parasitic side-lobe. The quantisation effects must also be taken into account, since these errors have an impact on the desired pre-defined side-lobe level envelope specification.

7. Conclusion:

PAF method consisting of a beamformer, low-noise amplifiers, an array feed with several mutually-coupled antenna parts, and an electrically large reflector has been modelled using a numerical technique. The simulated and observed beam sensitivities coincide rather well; that is, the percentage difference between the simulations and measurements is less than 11% for 31 beam orientations and roughly 30% for beams in center as well as borders of field of view (FOV). This is a good result considering complexity of methods as well as fact that the model does not take reflectorfeed interactions or the real feed box environment into consideration. As far as the authors are aware, this is the best consensus that the PAF community has seen thus far for a system this complicated. For tetrahertz medical imaging applications, circular polarised ring resonator microstrip patch antennas with graphene loads or photoconductive dipoles are to be used in the design of the 2 × 2 and 3 × 3 antenna arrays. The array has yielded results that meet the design parameters in terms of high peak power, directional gain, low sidelobe level, low average sidelobe level, angular resolution. Observed values indicate that the C-Band scanning range, over frequency bandwidth better than 500MHz, PT>20W per element, HPBW <-30dB, gain>30dB, and ASLL <-42dB.

Reference:

[1] Xu, L., Bi, S., Liu, J., Yuan, C., Zhang, Q., & Sun, Y. (2022). A phase synthesis method for reflectarray in high-power microwave application. *IEEE Transactions on Plasma Science*, *50*(9), 2858-2863.

[2] Prasad, S., Meenakshi, M., Adhithiya, N., Rao, P. H., Krishna Ganti, R., & Bhaumik, S. (2021). mmWave multibeam phased array antenna for 5G applications. *Journal of Electromagnetic Waves and Applications*, *35*(13), 1802-1814.

[3] Takabayashi, N., Kawai, K., Mase, M., Shinohara, N., & Mitani, T. (2022). Large-scale sequentially-fed array antenna radiating flat-top beam for microwave power transmission to drones. *IEEE Journal of Microwaves*, *2*(2), 297-306.

[4] Eid, Alla M., Ahmed Alieldin, Abdelrahman M. El-Akhdar, Ahmed F. El-Agamy, Walid M. Saad, and Amgad A. Salama. "A novel high power frequency beam-steering antenna array for long-range wireless power transfer." *Alexandria Engineering Journal* 60, no. 2 (2021): 2707-2714.

[5] Lu, P., Wagih, M., Goussetis, G., Shinohara, N., & Song, C. (2023). A comprehensive survey on transmitting antenna systems with synthesized beams for microwave wireless power transmission. *IEEE Journal of Microwaves*.

[6] Mackay, A. J., & Eleftheriades, G. V. (2023). Power pattern synthesis with peripherally excited phased arrays. *IEEE Transactions on Antennas and Propagation*, *71*(8), 6390-6398.

[7] Pauliah Nadar, K., Jeyaprakasam, V., Tharcis Mariapushpam, I., Vivekanand, C. V., Eswaralingam, A. D., Louis, M. T., ... & Gopalakrishnan, S. (2023). Design and Analysis of Microstrip Patch Antenna Array and Electronic Beam Steering Linear Phased Antenna Array with High Directivity for Space Applications. *ACS Omega*, *8*(45), 43197-43217.

[8] Arun, M., & Jebarani, M. E. (2023). Design of phased array antenna with low side lobes. *Materials Today: Proceedings*, *80*, 2150-2154.

[9] Kedar, A., Bisht, A. S., Sreenivasulu, K., Rao, D. S., & Vishwakarma, N. K. (2020, April). GaN based wide band C-band active phased array antenna design with wide scan volume. In *2020 IEEE International Radar Conference (RADAR)* (pp. 88-93). IEEE.

[10] Bang, J., & Choi, J. (2020). A compact hemispherical beam-coverage phased array antenna unit for 5G mm-wave applications. *IEEE Access*, *8*, 139715-139726.

[11] Su, Z. L., Leung, K. W., & Lu, K. (2022). A shaped-beam antenna for wide-angle scanning phased array. *IEEE Transactions on Antennas and Propagation*, *70*(9), 7659-7669.

[12] Vilenskiy, A. R., Liao, W. C., Maaskant, R., Vassilev, V., Iupikov, O. A., Emanuelsson, T., & Ivashina, M. V. (2021). Co-design and validation approach for beam-steerable phased arrays of active antenna elements with integrated power amplifiers. *IEEE Transactions on Antennas and Propagation*, *69*(11), 7497-7507.

[13] Xu, L., Yuan, C., Zhang, Q., Liu, J., Zhang, Q., & Sun, Y. (2023). Design and experiments of a beam-steerable wideband reflectarray antenna for high-power microwave applications. *IEEE Transactions on Antennas and Propagation*, *71*(2), 1955-1959.

[14] Xu, L., Ge, X., Zhang, Q., Dang, F., Zhang, P., Liu, J., & Yuan, C. (2023). A Beam-Steerable Wideband Reflectarray Antenna for C-Band High-Power Microwave Application. *IEEE Access*, *11*, 64559-64566.

[15] Kong, G., Li, X., Wang, Q., & Zhang, J. (2020). A wideband reconfigurable dual-branch helical reflectarray antenna for high-power microwave applications. *IEEE Transactions on Antennas and Propagation*, *69*(2), 825-833.

[16] Venkatesh, V., Orzel, K., & Frasier, S. (2020). Spaced-antenna aperture synthesis using an X-band active phased-array. *IEEE Geoscience and Remote Sensing Letters*, *18*(7), 1194-1198.

[17] Wei, C. Y., Zhang, H. C., He, P. H., Yan, X. T., Lu, J., & Cui, T. J. (2022). A dual circularly polarized SIW-fed phased array antenna with wide-angle beam scanning range. *IEEE Transactions on Antennas and Propagation*, *70*(9), 7393-7402.

[18] Milias, C., Andersen, R. B., Jørgensen, T. H., Muhammad, B., Kristensen, J. T., Mihosvka, A., ... & Zaharis, Z. D. (2023). Mechanically controlled, wide-angle scanning, series-fed antenna array with low profile for high-power radar systems. *IEEE Transactions on Antennas and Propagation*, *71*(8), 6454-6469.

[19] Eid, A. M., Alieldin, A., El-Akhdar, A. M., El-Agamy, A. F., Saad, W. M., & Salama, A. A. (2021). A novel high power frequency beam-steering antenna array for long-range wireless power transfer. *Alexandria Engineering Journal*, *60*(2), 2707-2714.